Alignment of the Cell Nucleus From Labeled Proteins Only for 4D In Vivo Imaging

B. RIEGER,[1]* C. MOLENAAR,[2] R.W. DIRKS,[2] AND L.J. VAN VLIET[1]
[1]*Quantitative Imaging Group, Faculty of Applied Sciences, Delft University of Technology, Lorentzweg 1, 2628 CJ Delft, The Netherlands*
[2]*Leiden University Medical Center, Department of Molecular Cell Biology, Laboratory for Cytochemistry and Cytometry, Wassenaarseweg 72, 2300 RA Leiden, The Netherlands*

KEY WORDS motion registration; confocal microscopy; time series

ABSTRACT Studies of protein dynamics by 4D (3D + time) confocal microscopy in vivo are hampered by global cell motion. The time between the acquisitions of the 3D images is in the order of minutes. Therefore, it is not to be expected that the cell as a whole remains fixed in the water basin on the stage. This superimposes a motion on the protein dynamics that has to be removed. We present a robust registration technique to align the cell images that does not require the a priori establishment of point-to-point correspondences. Instead, it uses the distribution of the labeled proteins. After correction for the translation, the 3D rotation of the cell is estimated. A robust intrinsic body coordinate system is constructed via the inertia tensor from the intensity distribution. By combining basis transformation to this intrinsic coordinate system, we can calculated the rotation matrix in a conceptual and computational straightforward manner. We have evaluated the performance of this approach in three experiments with human osteaosarcoma cells (U-2 OS), where the nuclear proteins Histon H4 and PML were visualized. The PML is concentrated in several dozen nuclear spots. Expression of Histon H4 results in a total nuclear staining. The registration results for both channels computed independently are very similar. Practically, this means that only the labeled material needs to be observed and still registration of the cell as a whole can be achieved. *Microsc. Res. Tech. 64:142–150, 2004.*

INTRODUCTION

Nowadays, confocal microscopy is used for the quantitative 4D imaging of spatiotemporal processes in living cells. The transport of proteins in the cell during the cell cycle is presumably a process that plays a role in RNA transcription and DNA repair (Dirks et al., 1999). Fluorescent labeling of such a protein reveals tens of moving spots in the cell. This motion, however, is superimposed on the translation and rotation of the cell as a whole. Here we propose a fully automatic method to remove this superimposed motion without first establishing point-to-point correspondence. After removing the global motion, the protein transport can be analyzed. The correction method is robust against noise and different axial and lateral resolution typical for confocal microscopy.

Acquisition and analysis of 4D image data (x, y, z, t) is an important tool in molecular cell biology to study the function of certain proteins in dynamic cellular processes (Brock and Jovin, 2003; Molenaar et al., 2003). Fluorescent labeling facilitates 4D imaging of specific proteins using confocal microscopy. The targets show up as moving bright spots. Often their velocity, absolute or with respect to each other, is of interest (Bergsma et al., 2001). Superimposed on the spot motion itself is the motion of the cell nucleus during the acquisition time (typically 30–120 minutes). We have developed an automatic procedure to estimate and remove the superimposed motion without the need to establish correspondence. The affine motion can be separated into translation and rotation (Scheck, 1999). First, the translation is estimated via the center of mass motion and, second the rotation parameters are estimated by constructing an intrinsic body system in each time frame via the inertia tensor. Both techniques work on the grey-value information of the image and do not require tracking or segmentation. The construction of an intrinsic body system via the inertia tensor has the big advantage that the rotation in 3D does not need to be done via the Euler angles. To compute the rotation matrix from two given systems via the Euler angles is conceptually complex. A generic 3D rotation $\mathbf{R}$ consists of three consecutive rotations in a 2D plane around the normal axis. The generic rotation $\mathbf{R} = \mathbf{R}_1\mathbf{R}_2\mathbf{R}_3$ obtained by matrix multiplication is not commutative, requiring an iterative one-by-one method to estimate the rotation angles. It is much easier to calculate the rotation matrix by combining the basis transformation in two time frames to a unique intrinsic coordinate system induced by the inertia tensor.

Often the correction for the cell motion is done by hand or by an algorithm that requires segmentation and matching of the objects. Pei and Liou (1994) have

*Correspondence to: Bernd Rieger, Quantitative Imaging Group, Faculty of Applied Sciences, Delft University of Technology, Lorentzweg 1, 2628 CJ Delft, The Netherlands. E-mail: rieger@ph.tn.tudelft.nl

Received 23 February 2004; accepted in revised form 15 May 2004

Contract grant sponsor: The Netherlands Organization for Scientific Research; Contract grant numbers: 612-012-003, 901-34-144.

DOI 10.1002/jemt.20069

Published online in Wiley InterScience (www.interscience.wiley.com).

presented another correspondences-less approach where they obtain the motion parameters via various order moments. However, they cannot give a confidence measure if the algorithms fails. For symmetric bodies, they fall back to a correspondence-based approach. Our algorithm can automatically detect symmetric body constellations (for which the body system is not unique). As long as the body is not a sphere, we can reduce the problem's dimensionality and solve the rotation by an explicit 2D rotation, which is easily characterized by only one angle. Again we can avoid the conceptual difficult Euler angles.

The goal of our approach is to compute the overall cell motion by observation of the protein motion only. The hypothesis that we need to check is: do the labeled protein spots move approximately the same as the cell nucleus (counterstain)? The motion of the counterstain and spots cannot be entirely correlated as the spots have an interesting biological function that we want to study. To test the hypothesis, we acquire protein spots and the cell nucleus at the same time by using two different fluorescent markers and compute the motion parameter on both independently. If these parameters show good correspondence, we can conclude that our approach is suitable. Furthermore, we want to study the effect of the correction on the motion trajectories of the spots. An accelerated motion of the cell should be visible via a curved spot trajectory in 4D before correction and a more straight trajectory after correction.

THEORY OF MOTION PARAMETER ESTIMATION

Using techniques based on the intensity of the image, we are going to retrieve the motion parameters of the affine transformation of the overall body motion without establishing correspondence of special points. We assume that only a single structure of interest, i.e., one cell, is in the field of view during the acquisition time. Furthermore, shifting and rotating the acquired 3D time series is computationally complex if the voxels are anisotropic, which is often the case in confocal microscopy as the lateral resolution is about 3–5 times higher than the axial. Therefore, as a preprocessing step the data are resampled to make the voxels isotropic.

Translation

If no movement of the individual spots occurs and only movement due to drift of the cell nucleus occurs, then the motion of the center of mass of the spot image perfectly characterizes the drift. Biological mass (protein/DNA) in images is identified through the intensity values $I(x)$ of the measured fluorophores. As long as the displacement of individual spots between two successive time frames is small, the center of mass will not be effected significantly, as the number of bright spots is large. The center of mass is calculated in each time frame

$$x_{CM} := \frac{1}{\sum I(x)} \sum I(x)x. \tag{2.1}$$

After computation of the x_{CM} for all time frames, we impose a shift on all images such that their x_{CM} coincide. We choose to shift all x_{CM} to the image center. This ensures that we keep maximal distance of the cell body to the images boundaries. For image processing purposes, it is desirable to avoid border effects of filtering operation, which is practically achieved by a distance of about 3 filter sizes of the object from the border (at a distance of 3σ, the Gaussian filters will only be marginally influenced by the border).

After subtracting the center of mass motion, we will correct for the rotation, which is the second step in this registration technique.

Rotation

A suitable way to find the rotation of a body without identifying special points and track them in time, is to construct a unique intrinsic coordinate system of the body at every time step. Such a system is induced by the principal axes of the inertia tensor (Scheck, 1999)

$$J_{\mu\nu} := \frac{1}{\sum I(x)} \sum I(x) \cdot (x^2\delta_{\mu\nu} - x_\mu x_\nu), \tag{2.2}$$

where the coordinate origin is the center of mass and $\delta_{\mu\nu}$ is the Kronecker-delta (Bronstein et al., 1999). The inertia tensor for images is normalized by the sum of the grey-values in contrast to the inertia tensor used in classical mechanics (Jähne, 1997; Scheck, 1999). The inertia tensor is real, symmetric, and positive. Therefore, it can be diagonalized by an orthonormal transformation $\mathbf{D} \in \mathrm{SO(n)}$ as

$$\mathbf{DJD}^{-1} = \bar{\mathbf{J}}, \tag{2.3}$$

where $\bar{\mathbf{J}}$ is diagonal. The eigenvectors of $\mathbf{J}$ form an orthogonal system and are called *principal axes*. Furthermore, the eigenvalues of $\mathbf{J}$ have the following property: $\lambda_i \geq 0$ and the sum of any two eigenvalues is greater or equal than the remaining one. We assume that $\bar{\mathbf{J}}$ can be considered constant between two successive time frames. The rotation between two time frames t and $t + 1$ of a group of objects described by their inertia tensor can be formulated with a rotation matrix $\mathbf{R} \in \mathrm{SO(n)}$ as

$$\mathbf{RJ}_t\mathbf{R}^{-1} = \mathbf{J}_{t+1} \tag{2.4}$$

In 3D, one or two rotations around some axes are in general not enough to let an object coincide. A possible way is the formulation by Euler angles as

$$\mathbf{R} = \mathbf{R}_{3''}(\gamma)\mathbf{R}_{2'}(\beta)\mathbf{R}_3(\alpha). \tag{2.5}$$

The first rotation is about angle α around the initial 3-axis. The second about angle β around the intermediate 2-axis, and the last about angle γ around the final 3-axis. The intervals for the angles are $\alpha \in [0, 2\pi]$, $\beta \in [0, \pi]$, $\gamma \in [0, 2\pi]$ (Scheck, 1999).[1] Solving eq. (2.4) for $\mathbf{R}$ and the three Euler angels in closed-form is not feasible with this rotation matrix

[1]There is another definition of the Euler angles. The second rotation is then about the intermediate 1-axis. The angles are called ψ, θ, ϕ and their relation with the other angles is $\phi = \gamma - \pi/2 (\mathrm{mod}\ 2\pi)$, $\theta = \beta$, $\psi = \alpha + \pi/2 (\mathrm{mod}\ 2\pi)$.

$$\mathbf{R} = \begin{pmatrix} \cos\gamma\cos\alpha - \cos\beta\sin\alpha\sin\gamma & \cos\gamma\sin\alpha + \cos\beta\cos\alpha\sin\gamma & \sin\beta\sin\gamma \\ -\sin\gamma\cos\alpha - \cos\beta\sin\alpha\cos\gamma & -\sin\gamma\sin\alpha + \cos\beta\cos\alpha\cos\gamma & \sin\beta\cos\gamma \\ \sin\beta\sin\alpha & -\sin\beta\cos\alpha & \cos\beta \end{pmatrix} \tag{2.6}$$

Fortunately, we are in a situation where the matrix under consideration **J** is real and symmetric, so it can be diagonalized. For two time frames, t and $t + 1$, we compute

$$\mathbf{J}_t = \mathbf{D}_t^{-1}\bar{\mathbf{J}}\mathbf{D}_t \tag{2.7}$$

$$\mathbf{J}_{t+1} = \mathbf{D}_{t+1}^{-1}\bar{\mathbf{J}}\mathbf{D}_{t+1}. \tag{2.8}$$

Solving for $\bar{\mathbf{J}}$ we get

$$\mathbf{J}_{t+1} = \mathbf{D}_{t+1}^{-1}\mathbf{D}_t\mathbf{J}_t\mathbf{D}_t^{-1}\mathbf{D}_{t+1}. \tag{2.9}$$

The overall rotation matrix is

$$\mathbf{R} = \mathbf{D}_{t+1}^{-1}\mathbf{D}_t. \tag{2.10}$$

For the actual computation, we can use the orthogonality of **R** and **D**. This a major advantage over the use of classical Euler rotation. This trick is only applicable where an intrinsic body system can be constructed at each time frame independently.

Degeneration of the Eigenvalue System: A Confidence Measure for Correspondence

The computation of the rotation matrix **R** is unique as long as the eigenvalue system of **J** is not degenerated. Let $\lambda_1 \geq \lambda_2 \geq \lambda_3 \geq 0$ be the eigenvalues of **J** and $\lambda_2 + \lambda_3 \geq \lambda_1$ due to the definition of the inertia tensor. We propose a normalized measure to indicate degeneration as

$$c_{deg} = \frac{\min(\lambda_1 - \lambda_2, \lambda_2 - \lambda_3)}{\lambda_1/3} \in [0,1]. \tag{2.11}$$

Where $c_{deg} = 1$ indicates maximal variance in the distribution of the eigenvalues and $c_{deg} \searrow 0$ indicates degeneration. The confidence measure can be interpreted geometrically. Imagine the λ_i's as distances in Euclidean space, then the condition

$$\lambda_i + \lambda_j \geq \lambda_k,\ i, j, k \in \{1, 2, 3\}\text{cyclic}, \tag{2.12}$$

is the triangle inequality, where $c_{deg} \searrow 0$ indicates symmetry of the triangle constructed by the line segments of length λ_i, as $c_{deg} \nearrow 1$ the triangle becomes more "asymmetric."

As long as λ_1^t corresponds to the same axis as λ_1^{t+1}, etc., the rotation is computed correctly. If the initial eigensystem is not degenerated, then the correspondence can only be broken by a transition via degenerated state, which we can detect.

If the body is truly symmetric, and not only the inertia, then for registration purposes it does not matter how the body axes are chosen. If the inertia is symmetric (twofold degeneration) but the distribution of the spots is not, then we can resolve the ambiguous coordinate system as follows. We project all spots onto the symmetry plane reducing the dimensionality of the problem to 2D. By cross-correlation, grey-value difference, 2D inertia tensor, or Fourier-Mellin analysis (Chen et al., 1994; Srinivasa Reddy and Chatterji, 1996) applied in this symmetry plane on two successive time frames, we obtain a 2D rotation angle about the symmetry axis. The use of Euler angles is again circumvented by projection and easy 2D rotation.

Stability of the Eigenvalue Analysis

Numerical eigenvalue analysis of noisy data is, in general, not very robust. In our cases the direction of corresponding eigenvectors in subsequent time frames should not flip. A flip can be detected via the sign of the volume spanned by the eigen system $\{v_i\}$ of **J**, i.e., $sgn(\det(\{v_i\}))$. To stabilize the computed eigen system, we require the system to have the same orientation for all time frames, i.e., either left- or right-handed.

Rotation of Images

We want the rotation point of a 3D image to be the center of mass that we fixed in Translation to be the image center. The easiest way to do this is by translation of the image about a vector v. A well-known formalism in computer graphics to combine a translation, rotation, and another translation into one matrix operation is through the concept of the *homogeneous coordinates* (Hearn and Baker, 1997). The translation can be expressed in a matrix by

$$\mathbf{T} = \begin{pmatrix} 1 & 0 & 0 & -v_x \\ 0 & 1 & 0 & -v_y \\ 0 & 0 & 1 & -v_z \\ 0 & 0 & 0 & 1 \end{pmatrix}, \quad \tilde{\mathbf{T}} = \begin{pmatrix} 1 & 0 & 0 & v_x \\ 0 & 1 & 0 & v_y \\ 0 & 0 & 1 & v_z \\ 0 & 0 & 0 & 1 \end{pmatrix} \tag{2.13}$$

The rotation matrix R is expanded into a 4×4 matrix

$$\hat{\mathbf{R}} = \begin{pmatrix} & & & 0 \\ & \mathbf{R} & & 0 \\ & & & 0 \\ 0 & 0 & 0 & 1 \end{pmatrix}. \tag{2.14}$$

Combining these matrices, the transformation of an old vector $(x, y, z)^t$ to a new vector $(x', y', z')^t$ becomes

$$\begin{pmatrix} x' \\ y' \\ z' \\ . \end{pmatrix} = \bar{\mathbf{T}}\hat{\mathbf{R}}\mathbf{T}\begin{pmatrix} x \\ y \\ z \\ . \end{pmatrix}. \tag{2.15}$$

For a rotation around the center of the image, the translation vector chosen must be half the image size.

The actual application to an image requires some more steps due to the quantization of the image. For a given voxel in the output image, there is in general no associated voxel in the input image, so that value must be obtained through interpolation. Different methods of interpolation are known in the literature, as linear (first order hold), bispline, cubic, etc. In our case, the simplest and fastest of them (linear) turned out to be sufficient.

Measure for Rotations

The Euler angles do not give an easy interpretation of how much an object is rotated. More intuitive measures for the degree of rotation are the rotation matrix **R** and the angles between corresponding pairs of eigenvectors of the inertia tensor **J**. For the rotation matrix, the deviation from the unit matrix defines a measure for rotation. For the eigenvectors of **J**, the angles give a very good measure for the rotation.

MATERIALS AND METHODS

Three time series of 15 time frames each were recorded in a time-span of about one hour. The image has two channels for two nuclear proteins (channels). The 3D images are of size $256 \times 256 \times 31$ voxels with a physical voxel size of $148 \times 148 \times 244$ nm and were recorded with 8-bit integer resolution. The cells are not spheres in this development stage, but rather flat, comparable to a bread dough before rising. The cell is captured in an image of about $38 \times 38 \times 8$ μm. One protein (H4-CFP) is distributed over the cell nucleus, which we will refer to as counterstain. The other one (PML-YFP) is localized at distinct spots (see Fig. 1). The acquisition of the counterstain along with the spots in another channel enables us to test our correction algorithm.

Two nuclear proteins were visualized in the living cells: Histon H4 and PML. The DNA-helix in eukaryotic cells is highly condensed. The first degree of packaging is formed by nucleosomes. About 146 base pairs are wrapped around protein octamers containing two copies of each of the four core histones, H2A, H2B, H3, and H4. The H3-H4 tetramer forms the inner core of the nucleosomes and these proteins are stable bound to DNA. The PML protein is typically found concentrated in 20–50 discrete nuclear spots, called PML bodies. The PML body has been associated with several human disorders, such as acute promyelocytic leukemia and AIDS. The molecular functions of PML bodies are not completely understood, but have been ascribed roles in RNA transcription/transport and DNA repair/replication. Using DNA-recombinant techniques, two auto fluorescent (AFP) fusion proteins were constructed, Histon H4-CFP and PML-YFP, and expressed in human osteaosarcoma cells (U-2 OS). The chimeric proteins mimic the function and localization of the endogenous proteins and enable dynamic live cell imaging. Expression of Histon H4-CFP results in a total nuclear staining and expression of PML-YFP in staining of about 30 PML bodies.

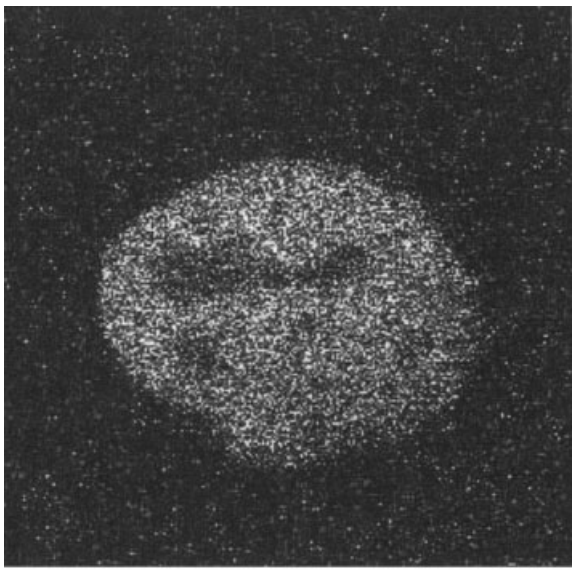

(a)

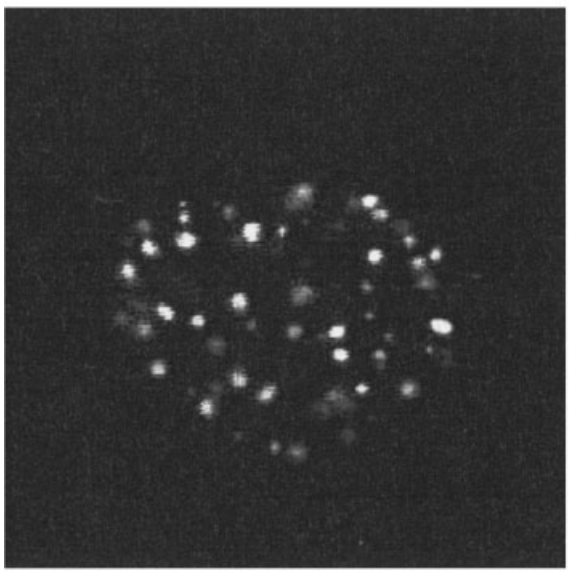

(b)

Fig. 1. **a:** Counterstain H4-CFP. **b:** Spots PML-YFP at time frame 8, z-slice 25.

Methods: Cloning of GFP-Fusion Proteins

The cDNAs encoding PML and Histon H4 were generated by RT-PCR on cDNA copied from mRNA isolated from human U-2 OS cells and cloned into the pECFP-C1 or pEYFP-C1 vectors (Clontech, Palo Alto, CA).

Live Cell Imaging

The AFP-fusion proteins were transiently expressed in U-2-OS cells using DOTAP (Roche Diagnostics

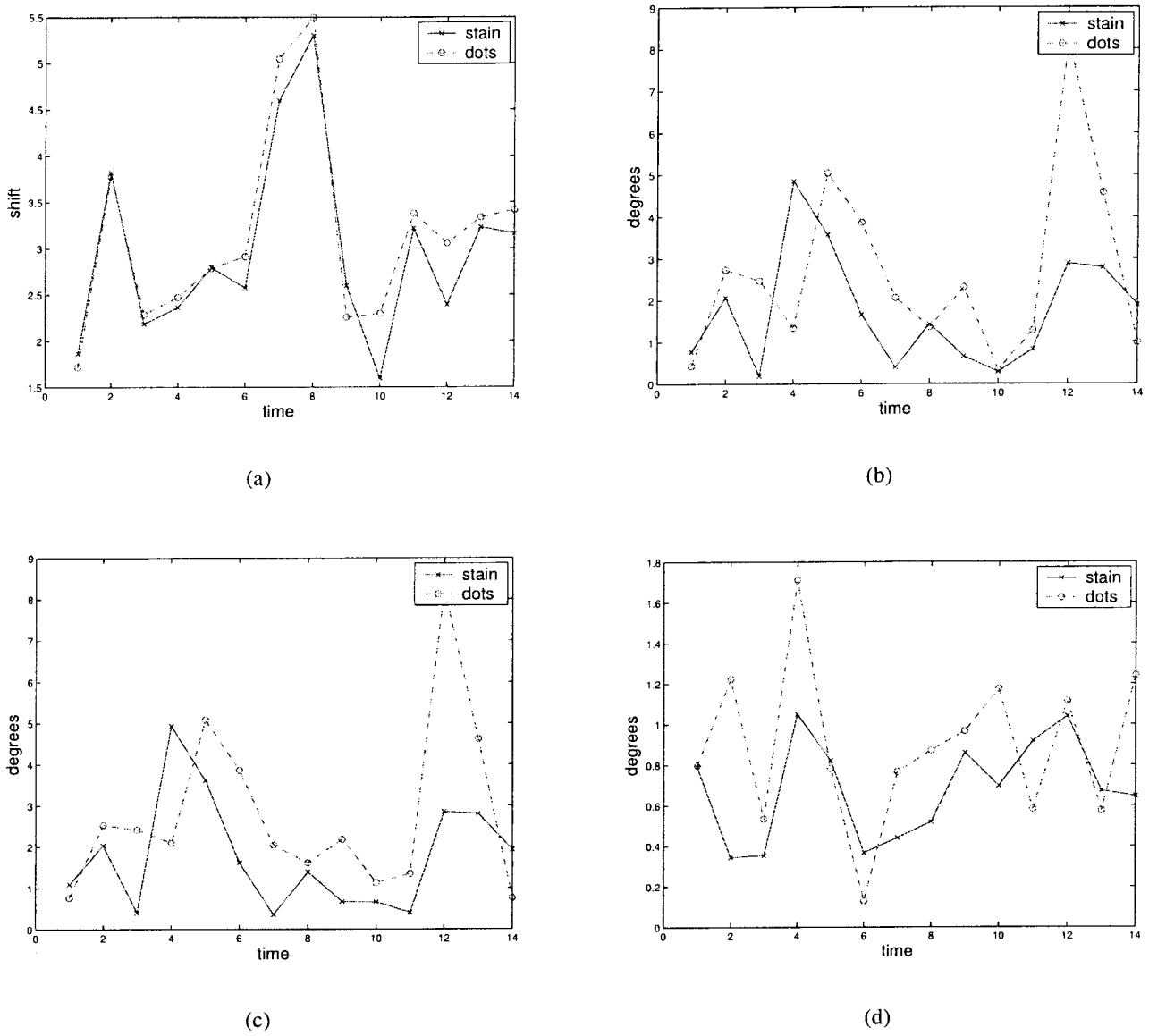

Fig. 2. Series 1: **(a)** Shift of the center of mass in pixel; **(b)** rotation of the first eigenvector in degrees between time frames: rotation of the second **(c)** and third **(d)** eigenvector in degrees between time frames.

GmbH). Cells were analyzed 24–48 hours after transfection and were se lected for moderate expression and protein-specific localization. The temperature of the cells was maintained at 37°C using a heated ring surrounding the culture chamber and a microscope objective heater (Bioptechs, Butler, PA). Images were acquired on a Leica TCS/SP2 confocal microscope system using a 100× NA 1.4PL APO lens. The 457- and 514-nm lines of the Argon laser were used for, respectively, CFP and YFP excitation. CFP and YFP were sequentially scanned to avoid cross-talk through the emission window.

RESULTS

For all three time series and in both channels, the degeneration measure (2.11) is $c_{deg} > 0.75\ \forall t$, i.e., there is no transition via a symmetrical state. This indicates that our approach is valid under real circumstances. In Figure 2, 4, and 6a, we have plotted the computed center of mass shift for the three time series for the counterstain and the spots. The rotation of the eigenvectors is depicted in Figures 2, 4, and 6b–d. The shift estimate of the counterstain and spots is in very good agreement. The overall shift is shown in Table 1. The rotation of corresponding eigenvectors between time frames is also well correlated. Therefore, it is reasonable to say that the motion parameters of the whole nucleus can be computed from the spots only, if they are distributed over the whole cell. We notice a short time lag in rotation (depicted by the shifted peaks). The actual lag cannot

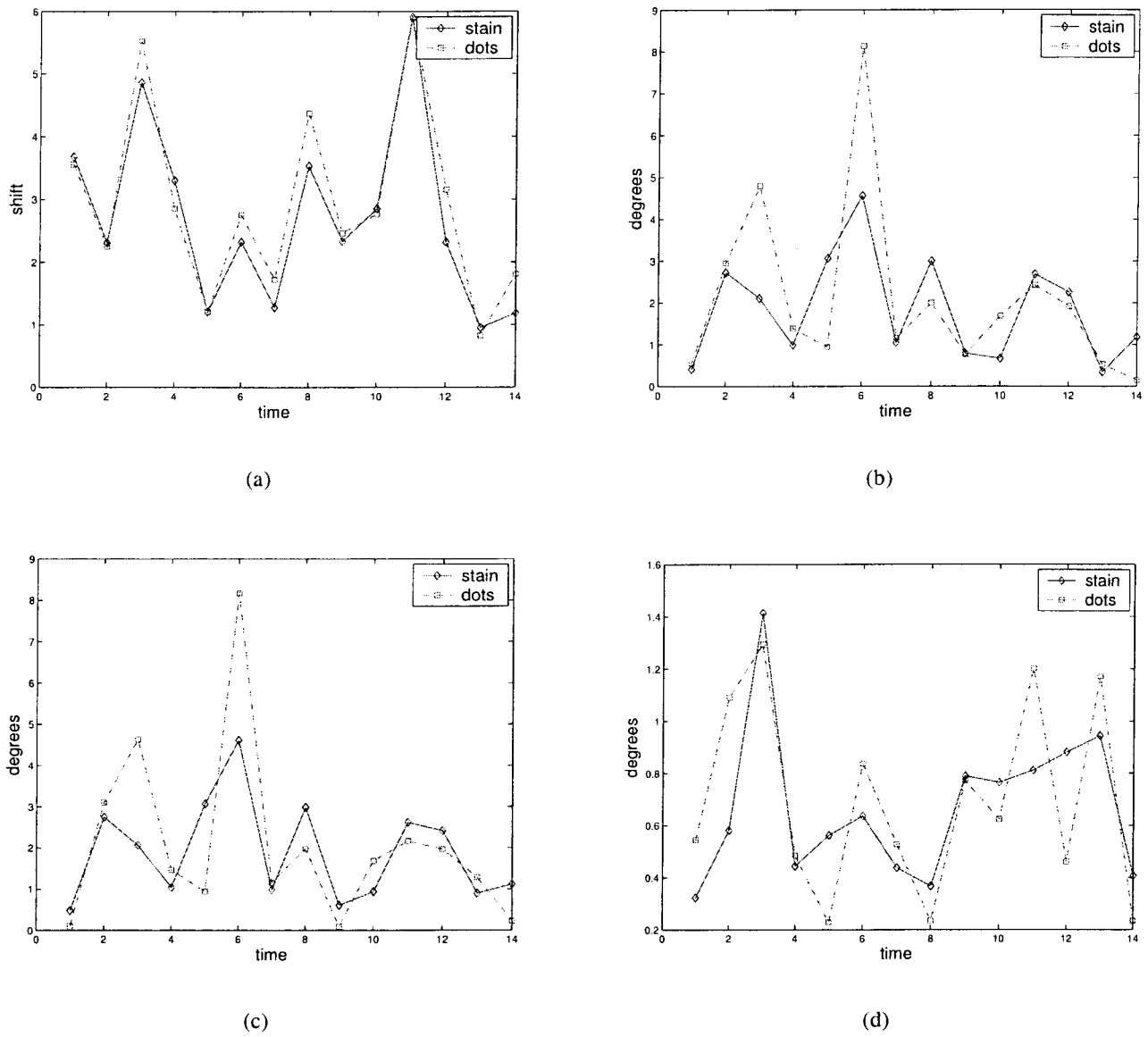

Fig. 3. Series 2: **(a)** Shift of the center of mass in pixel; **(b)** rotation of the first eigenvector in degrees between time frames; rotation of the second **(c)** and third **(d)** eigenvector in degrees between time frames.

be estimated due to the coarse time sampling. Another noticeable difference between the counterstain and spot rotation angles is the higher amplitude of the counterstain rotation. These higher amplitudes can be caused by shape differences of the cell that have a high impact on the estimated pose. More important, it is not to be expected that the spot and counterstain rotation is exactly the same. The spots move within the cell, but perform a motion correlated to their biological activity, which we want to study. Even stronger, if the counterstain and the spot motion would not differ at all, then the labeled spots would not have a interesting biological function, as they just stand still inside the nucleus. In Table 2, we show the computed correlation between the counterstain and spots rotation of the different eigenvectors. We compute the correlation as the cosine of the angle between the vectors and as the normalized difference between the vectors formed by the rotation angle of the eigenvectors of the counterstain and the spots (plotted in Figs. 2, 4, and 6b–d).

Furthermore, we see a strong correlation between the motion of the first v_1 and second eigenvector v_2 in Figures 2, 4, 6b, c. They rotate more than v_3 in Figure 2, 4, and 6d. The correlation between the v_1 and v_2 rotation comes from the flat shape of the cell. A typical cell is 4–5 times wider than high after preparation. Based on this shape of the cell, we conclude therefore: v_1 and v_2 lie approxi-

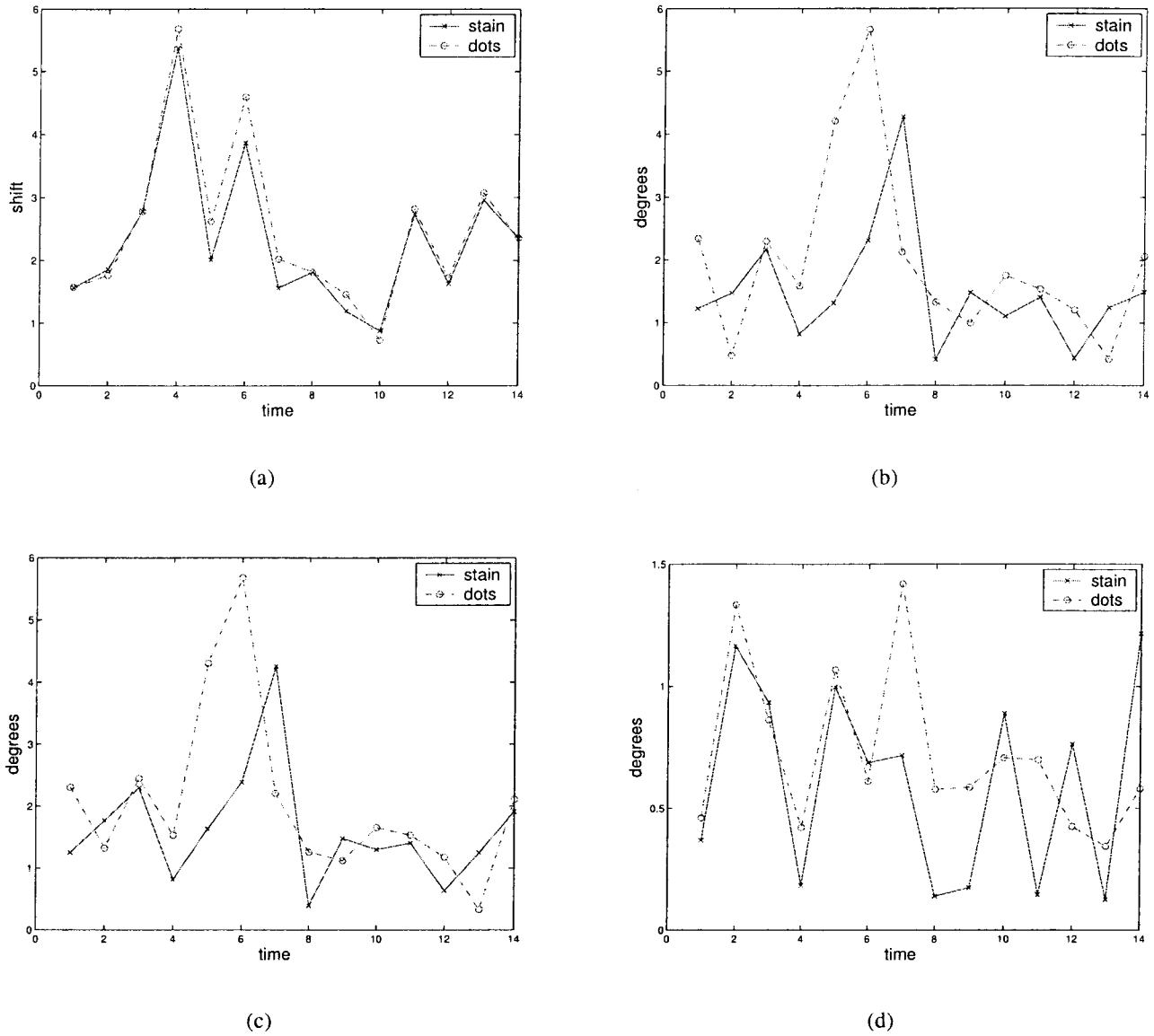

Fig. 4. Series 3: **(a)** Shift of the center of mass in pixel; **(b)** rotation of the first eigenvector in degrees between time frames; rotation of the second **(c)** and third **(d)** eigenvector in degrees between time frames.

TABLE 1. Total shift of the center of mass computed form the counterstain and the spot channels[1]

	Shift counterstain (μm)	Shift spots (μm)	$\bar{c}_{1D}$ before	$\bar{c}_{1D}$ after
Series 1	3.32	3.53	0.145	0.175
Series 2	4.32	4.31	0.145	0.187
Series 3	2.52	2.56	0.142	0.191

[1]The mean confidence $\bar{c}_{1D}$ before and after the correction.

TABLE 2. Correlation between the spots and counterstain rotation for the different eigenvectors[1]

	Series 1		Series 2		Series 3	
	ρ	diff	ρ	diff	ρ	diff
corr(counterstain,spots) v_1	0.79	0.37	0.88	0.31	0.80	0.35
corr(counterstain,spots) v_2	0.81	0.36	0.88	0.34	0.83	0.32
corr(counterstain,spots) v_3	0.93	0.24	0.94	0.24	0.89	0.24
corr(spots,spots) v_1, v_2	1.0	0.049	0.99	0.050	0.99	0.048

[1]Last row: Correlation between the first and second eigenvector of the spots. ρ: = $v_i(counterstain) \cdot v_i(spots)/\|v_i(counterstain)\| \|v_i(spots)\|$, *diff*: = $\|v_i(counterstain) - v_i(spots)\|/(\|v_i\ (counterstain)\ \| + \| v_i(spots)\|)$. A ρ close to one indicates good correlation.

mately in the *xy*-plane, i.e., the elongated direction of the cell, and v_3 close to the axial direction. Thus, the cell rolls little in the axial direction during acquisition compared to the rotation in the lateral plane.

4D Measures

The result of the cell body motion on the spots has been studied as follows: Before and after the motion parameter correction, we compute a 1D line-likeness measure in the 4D image of the spots. This measure indicates per pixel how certain it is that a spot trajectory is present here. No thresholding is done, but a

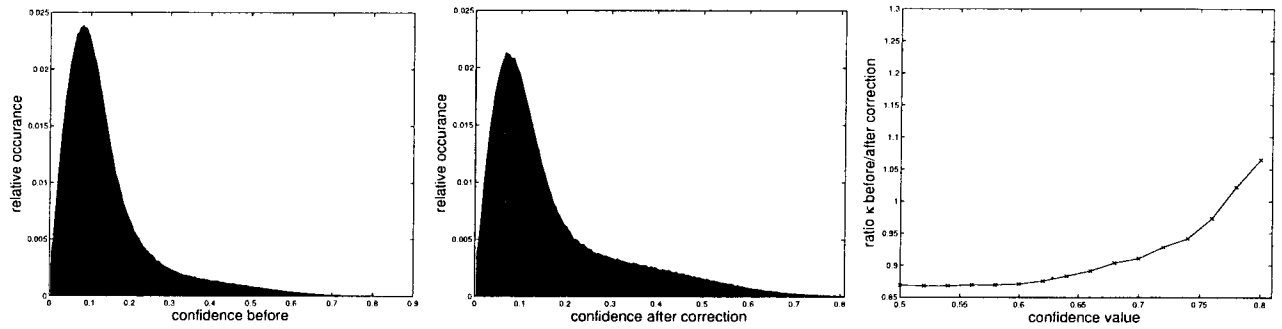

(a) (b) (c)

Fig. 5. Series 1: **(a)** Histogram of c_{1D} before correction, **(b)** after correction, **(c)** $\bar{\kappa}_{before}/\bar{\kappa}_{after}$ as a function of the regions with c_{1D} higher than the threshold.

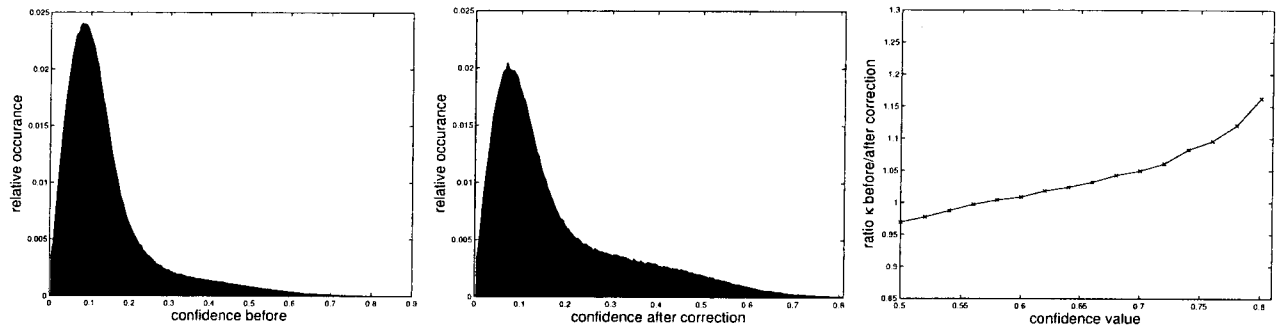

(a) (b) (c)

Fig. 6. Series 2: **(a)** Histogram of c_{1D} before correction, **(b)** after correction, **(c)** $\bar{\kappa}_{before}/\bar{\kappa}_{after}$ as a function of the regions with c_{1D} higher than the threshold.

high value of this measure indicates a spot trajectory, not only the presence of a spot in one image. We use

$$c_{1D} = \frac{l_3 - l_4}{l_3 + l_4} \in [0,1], \tag{4.16}$$

as a normalized measure (Kempen et al., 1999), where $l_i \geq l_{i+1} \geq 0$ are the eigenvalues of the gradient structure tensor (Bigün and Granlund, 1987; Kass and Witkin, 1987; Jähne, 1997; Kempen et al., 1999)

$$\bar{G} := \overline{\partial_\alpha I \partial_\beta I},\ \alpha, \beta = 1, \cdots 4 \tag{4.17}$$

applied to the 4D (x, t)-image. Here, the overhead bar denotes averaging over a local spatio-temporal neighborhood.

In Figures 3, 5, and 7, the histograms of the line-likeness confidence measures are shown (1) before and (2) after the correction. The peak position in the confidence histogram before and after correction does not change. However, notice the substantially increased tail of the distribution towards the high confidence values. This indicates that the path of the spots has been straightened with respect to the path before registration. We conclude that is due to the removal of the rotation, as there is no acceleration of the spots (see below). The mean confidence increases about 20% for all series (compare also Table 1).

Furthermore, we investigate the acceleration of the spots. A measure for the force and thereby the acceleration a is the curvature of the 4D spot trajectory (Frankel, 1997)

$$a = |\dot{v}|T + |v|^2 \kappa(s) N. \tag{18}$$

This is the classical expression of the tangential and the normal components of the acceleration. Here T is the local tangent to the trajectory, N the normal, and v the velocity, which can be computed, for example, with the help of optical flow (see Lucas and Kanade, 1981). The curvature is computed by an algorithm presented by Rieger and Vliet (2002), which is based on the grey-value distribution and avoids segmentation. In Figures 3, 5, and 7c, we show the ratio of the average curvature $\bar{\kappa}$ before and after the correction as a function of the regions with a least a certain line-likeness value c_{1D}. The mean curvature before and after correction as a function of the confidence increases only slightly for

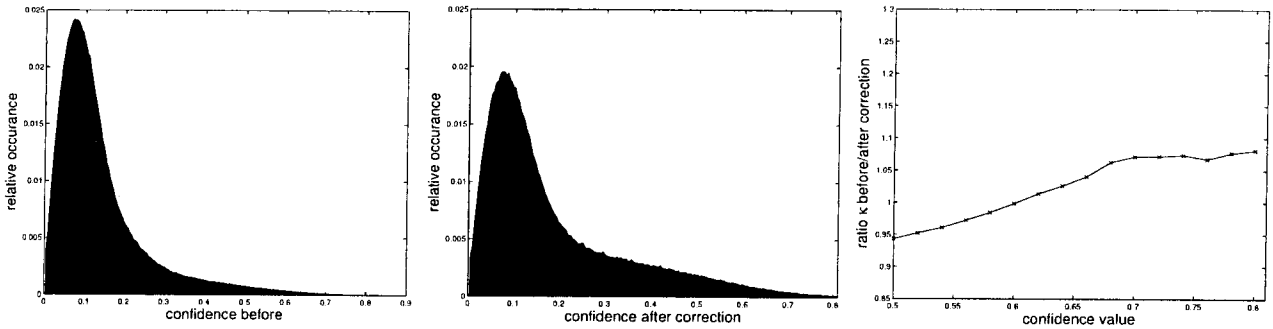

Fig. 7. Series 3: **(a)** Histogram of c_{1D} before correction, **(b)** after correction, **(c)** $\bar{\kappa}_{before}/\bar{\kappa}_{after}$ as a function of the regions with c_{1D} higher than the threshold.

higher confidences. Therefore, we conclude that the corrected motion is not accelerated. The cell does not roll on the stage as seen from the angles of the third eigenvector and the drift in the water basin seems to be force free.

DISCUSSION

We present a fully automatic algorithm to obtain motion parameters in 3D without establishing correspondence of individual points. The inertia tensor provides a robust intrinsic coordinate system in every time frame. This enable us to calculate the rotation matrix by combining basis transformations to this intrinsic system, instead of using the Euler angle formalism. A measure to detect failure of the rotation correction is presented (Eq. 2.11). The motion parameters can be reliably computed from the spots. If it is possible, the motion parameters of the counterstain observation should be used to correct the spot movement as the counterstain is not influenced by dislocations of labeled material. This automatic correction should be the first step in analyzing the relative motion of individual spots. It enables us to only observe the spots and at the same time to correct for the cell nucleus motion, which is an experimental advantage.

ACKNOWLEDGMENTS

This work was partially supported by the Netherlands Organization for Scientific Research, grant 612-012-003 (to B.R.) and grant 901-34-144 (to C.M.). Both authors of the NWO program "4D imaging of living cells and tissues." The calculations were performed with the MATLAB toolbox DIPimage (Luengo Hendriks et al., 1999), which is freely available for academic usage. The software for the protocol presented here can be obtained from the authors.

REFERENCES

Bergsma C, Streekstra G, Smeulders A, Manders E. 2001. Velocity estimation of spots in 3d confocal images sequences of living cells. Cytometry 43:261–272.

Bigün J, Granlund G. 1987. Optimal orientation detection of linear symmetry. Proceedings of the first IEEE International Conference on Computer Vision. London: IEEE Computer Society Press. p 433–438.

Brock R, Jovin T. 2003. Quantitative image analysis of cellular protein translocation induced by magnetic microspheres: application to the egf receptor. Cytometry Part A 52:1–11.

Bronstein I, Semendjajew K, Musiol G, Mühlig H. 1999. Taschenbuch der Mathematik, 4th ed. Thun, Frankfurt (Main): Verlag Harri Deutsch.

Chen Q, Defrise M, Deconinck F. 1994. Symmetric phase only matched filtering of Fourier-Mellin transforms for image registration and recognition. IEEE Transact Pattern Anal Machine Intell 16:1156–1168.

Dirks R, Hattinger C, Molenaar C, Snaar S. 1999. Synthesis, processing, and transport of RNA within the three-dimensional context of the cell nucleus. Crit Rev Eukaryot Gene Exp 9:191–201.

Frankel T. 1997. The geometry of physics. Cambridge: Cambridge University Press.

Hearn D, Baker M. 1997. Computer graphics, 2 ed. Englewood Cliffs, New Jersey: Prentice Hall.

Jähne B. 1997. Digital image processing, 4th ed. Berlin: Springer.

Kass M, Witkin A. 1987. Analyzing oriented patterns. Comput Vis Graph Image Process 37:362–385.

Kempen Gv, Brink Nvd, Vliet Lv, Ginkel Mv, Verbeek P. 1999. The application of a local dimensionality estimator to the analysis of 3d microscopic network structures. SCIA'99, Proc. 11th Scandinavian Conference on Image Analysis, Kangerlussuaq, Greenland. 447–455.

Lucas B, Kanade T. 1981. An iterative image registration technique with an application to stereo vision. In: Proceedings of the Seventh Int. Conf. on Artifical Intelligence. Hayes P, editor. Vancouver, Canada: William Kaufmann. p 674–679.

Luengo HC, Rieger B, Ginkel Mv, Kempen Gv, Vliet Lv. 1999. DIPimage: a scientific image processing toolbox for MATLAB. Delft University of Technology, http://www.ph.tn.tudelft.nl/DIPlib.

Molenaar C, Wiesmeijer K, Verwoerd N, Khazen S, Eils R, Tanke H, Dirks R. 2003. Visualizing telomere dynamics in living mammalian cells using PNA probes. EMBO J 22:6631–6641.

Pei S.-C, Liou L.-G. 1994. Using moments to acquire the motion parameters of a deformable object without correspondence. Image Vis Comput 12:475–485.

Rieger B, Vliet Lv. 2002. Curvature of n-dimensional space curves in grey-value images. IEEE Transact Image Process 11:738–745.

Scheck F. 1999. Mechanics: from Newton's law to deterministic chaos. Berlin: Springer.

Srinivasa Reddy B, Chatterji B. 1996. A fft-based technique for translation, rotation and scale-invariant image registration. IEEE Transact Image Process 5:1266–1271.